Dosage compensation and meiotic sex chromosome inactivation are maintained in the absence of selection

Darren J. Parker[1,2], Zoé Dumas[1], Rocío Gómez Lencero[3], Jean-Marc Aury[4], Marjorie Labedan[1], Patrick Tran Van[1], Benjamin Istace[4], Corinne Cruaud[5], Karine Labadie[5], Benjamin Noel[4], Susana Freitas[1], Jelisaveta Djordjevic[1], and Tanja Schwander[1]

1. Department of Ecology and Evolution, University of Lausanne, Lausanne, Switzerland.
2. School of Natural and Environmental Sciences, Bangor University, Bangor, UK.
3. Department of Biology, Universidad Autónoma de Madrid, Spain
4. Génomique Métabolique, Genoscope, Institut François Jacob, CEA, CNRS, Université Evry, Université Paris-Saclay, 91057 Evry, France
5. Genoscope, Institut François Jacob, CEA, CNRS, Université Evry, Université Paris-Saclay, 91057 Evry, France

Abstract

Dosage compensation (DC) and meiotic sex chromosome inactivation (MSCI) are key mechanisms regulating gene expression from the X chromosome in male-heterogametic species. While the convergent evolution of these mechanisms is well-documented, their evolutionary fate under relaxed selection remains poorly understood. Here, we test whether DC and MSCI persist in the absence of selection by investigating three independently derived parthenogenetic species of *Timema* stick insects that occasionally produce rare males. Using chromosome-level genome assemblies, RNA-seq from multiple tissues, and immunocytochemistry, we find that dosage compensation in somatic tissues and meiotic X inactivation are conserved despite the absence of selective pressure in all-female lineages. Surprisingly, expression data and cytological markers indicate that MSCI signatures are even stronger in parthenogenetic males, a pattern driven by prolonged autosomal transcription during meiosis. These results indicate that X-targeting DC and MSCI mechanisms are either weakly selected against or evolutionarily constrained, while autosomal mis-expressing during meiosis occurs rapidly following the relaxation of selection, shedding light on the stability of X chromosome regulation.

Introduction

Sexual reproduction is key to the diversity of life and the main driver of species' lifecycles. In eukaryotic species with distinct male and female sexes, sex determination is frequently governed by sex chromosomes such as X and Y chromosomes in male heterogametic species. Because males carry only a single X chromosome while females carry two, X chromosome expression is regulated by highly specialized mechanisms: dosage compensation (DC, in somatic cells) and meiotic sex chromosome inactivation (MSCI, in germ cells). DC is a mechanism that balances the expression of X-linked genes between sexes. It has evolved independently across a wide range of taxa (Disteche, 2012; Mank, 2013; Gu and Walters, 2017) including mammals (Brockdorff and Turner, 2015), reptiles (Marin *et al.*, 2017), fish (Darolti *et al.*, 2019; Metzger *et al.*, 2021), nematodes (Meyer, 2000), and insects (Prince *et al.*, 2010; Conrad and Akhtar, 2012; Vicoso and Bachtrog, 2015; Pal and Vicoso, 2015; Rayner *et al.*, 2021; Chauhan *et al.*, 2021; Parker *et al.*, 2022).

However, the X is typically not dosage compensated in gonads, where expression from the sex chromosome(s) is further often suppressed via MSCI (Disteche, 2012; Djordjevic et al., 2024; Mank & Ellegren, 2009; Rayner et al., 2021; Vicoso et al., 2013). Specifically, MSCI involves the inactivation of heteromorphic sex chromosomes during meiosis through the addition of repressive chromatin marks, likely due to the inability of the X and the degraded (or completely lacking) Y to synapse (Burgoyne et al., 2009). While far from ubiquitous (McKee and Handel, 1993; Mank, 2013), DC and MSCI are typically maintained across clades for millions of years. Furthermore, a breadth of studies on both mechanisms indicate that they can evolve convergently as new sex chromosomes arise, involving similar or different mechanisms. This is revealed for example by research in dipterans, where X chromosomes have emerged independently from ancestral autosomes, with different DC mechanisms emerging in parallel (Hamada *et al.*, 2005; Straub *et al.*, 2005; Pease and Hahn, 2012; Davis *et al.*, 2018; Krzywinska *et al.*, 2023; Kalita *et al.*, 2023; Kalita and Keller Valsecchi, 2024; Toups and Vicoso, 2025). Similarly, the independent evolution of MSCI mechanisms in divergent taxa involves both shared and lineage-specific components (e.g. (Namekawa and Lee, 2009; Schoenmakers *et al.*, 2009; Page *et al.*, 2023)).

In contrast to the evidence for the convergent *de novo* evolution of DC and MSCI, it remains unknown how ancestral DC and MSCI systems evolve once they become redundant, which would be the case upon the evolution of a novel sex chromosome system. This is in part because suitable model systems with sex chromosome turnovers and accompanying evolution of X-targeting regulatory mechanisms remain understudied. Furthermore, sex chromosome turnover events in species with established DC and MSCI systems are expected to be rare because the maintenance of active systems could cause extensive misregulation of gene expression on the newly-formed sex chromosomes (Kelley *et al.*, 1995; Lee, 2000; Toups and Vicoso, 2023). A unique opportunity to overcome such constraints is to study the fate and potential decay of DC and MSCI in all-female parthenogenetic species. Following a transition to parthenogenesis, the X chromosome effectively adopts an autosomal inheritance pattern as it no longer varies in copy numbers since all individuals are female and carry two X copies. As a result, if DC or MSCI is costly (because of the cost of the machinery or due to maladaptive expression in females) we would expect selection to reduce a species' ability to perform these mechanisms following a transition to parthenogenesis. Such a reduction is

difficult to observe in parthenogenetic species as we need to examine expression in both sexes. This barrier can be overcome in some systems if rare males are produced.

Here we take advantage of such rare males to examine dosage compensation and meiotic sex chromosome inactivation in three species of parthenogenetic *Timema* stick insects, using a combination of new chromosome-level genome assemblies, RNA sequencing of eight different tissues, and cell biology. *Timema* have had multiple independent transitions to parthenogenetic reproduction over the last 0.5-1.5 million years (Schwander and Crespi, 2009; Schwander *et al.*, 2011; Bast *et al.*, 2018; Jaron *et al.*, 2022). Previously we have found that sexual *Timema* species show complete dosage compensation in somatic tissues throughout development, and meiotic X chromosome inactivation in the male germline (Parker *et al.*, 2022; Dumas *et al.*, 2024; Djordjevic *et al.*, 2025). This targeted regulation of the X chromosome likely involves putative general “insect molecular toolkits” (Djordjevic *et al.*, 2025) given that the stick insect X chromosome likely evolved prior to the diversification of insects over 450 mya (Toups and Vicoso, 2023). We can examine changes in dosage compensation and meiotic sex chromosome inactivation in parthenogenetic *Timema* as they occasionally produce rare males via two different processes. Some males arise from aneuploidy of the X chromosome (Schwander *et al.*, 2013), which since *Timema* have an XX/X0 sex-determination system, results in the production of a male. Others develop as a consequence of very rare instances of sex within parthenogenetic populations (Freitas *et al.*, 2023). Contrary to our prediction we find that the targeted regulation of the X chromosome underlying DC and MSCI has been conserved in each of the three parthenogenetic lineages, with relaxed selection affecting autosomal rather than X-linked expression in male meiotic cells. These results indicate that selection against X-regulatory mechanisms is weak or that changes to DC and MSCI mechanisms are highly constrained.

Results and Discussion

Genome assemblies reveal a highly conserved X chromosome contrasted by autosomal fissions and fusions

We generated chromosome-level genome assemblies for two of the three sexual species of *Timema* used in this study, *T. cristinae* and *T. podura*, to complement the available assembly of *T. poppense* (Table S1). In both new assemblies, the number of large scaffolds assembled (hereafter referred to as chromosomes) matched previous karyotype information (Schwander and Crespi, 2009) and coverage of male- vs female-derived short reads were used to identify the X chromosome (Supplemental Info). Annotation using a combination of gene predictions, protein, and RNAseq evidence from each species and its parthenogenetic sister species and inference of 8118 one-to-one orthologs (see Methods) revealed that the X chromosome content has not changed in any of the sexual or asexual species, as expected given the long-term conservation of X chromosome content in stick insects (Simon et al., 2019; Parker et al., 2022). Using comparisons with a stick insect (*Bacillus rossius*) from the Euphasmatodea clade (which split over 120 million years ago from *Timema (Bank and Bradler, 2022)*, we further find that even X chromosome synteny is highly conserved, while many rearrangements are apparent on the autosomes (Fig. 1). Specifically, the change in karyotype from 14 to 12 chromosomes during *Timema* evolution (Schwander and Crespi, 2009) involved at least two fissions and three fusions involving *T. podura* chromosomes 2, 3, 5 and 10 (Fig. 1, S1).

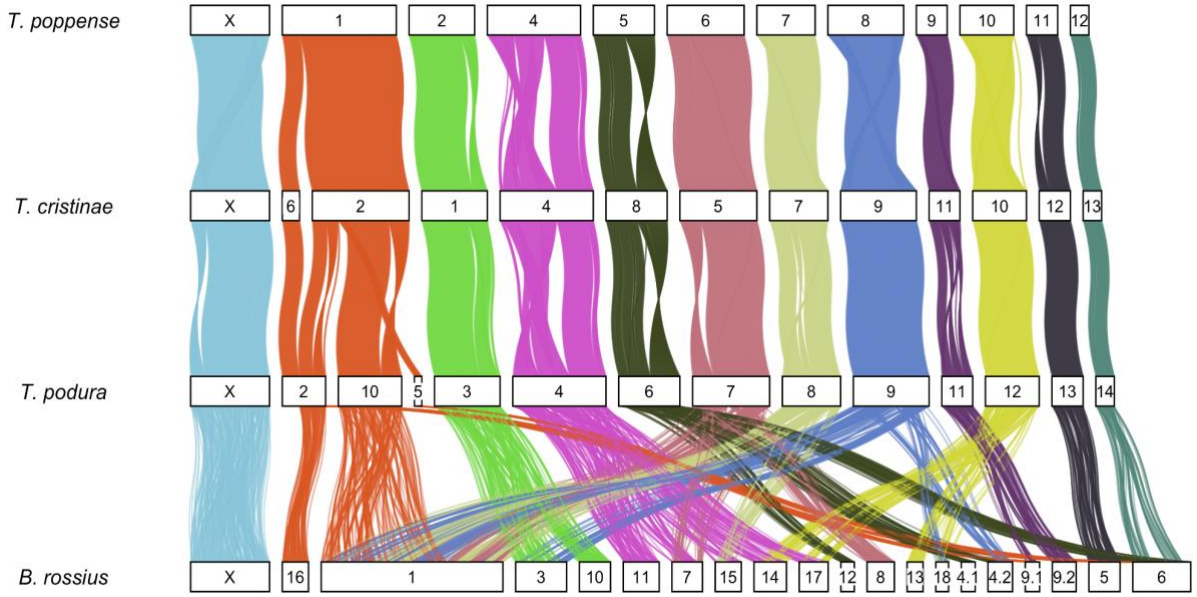

Fig. 1 | Autosomal genomic instability contrasts with X chromosome conservation. Chord diagram showing synteny between the assemblies based on 4241 one-to-one orthologs across the focal *Timema* genomes and a distantly related stick insect (*Bacillus rossius*). See Fig. S1 for synteny based on 8118 one-to-one orthologs across *Timema* only.

Dosage compensation in somatic tissues is not reduced in parthenogenetic species

Dosage compensation between the sexes in parthenogenetic species was very similar to that observed in sexual species. In all seven non-reproductive tissues (antennae, brain, defence glands, gut, fat body, femur, and tarsi) we observe almost complete dosage compensation in all species (Fig. 2). As expected, we observe some variation in the expression of X-linked genes between the sexes for specific tissues and species (resulting in small but significant differences in expression of autosomal versus X-linked genes). Such variation is typical in studies of dosage compensation (e.g., (Rayner *et al.*, 2021; Hu *et al.*, 2022; Li *et al.*, 2024) and can be interpreted as sex-specific regulation of individual genes rather than a consequence of variable or incomplete dosage compensation. If dosage compensation was reduced in parthenogenetic species, we would expect to see a larger deviation from complete dosage compensation in parthenogenetic species and an accompanying lower male-to-female expression ratio for the X in parthenogenetic species when compared to the sexual sister species for tissues with almost complete dosage compensation. We do not observe this, instead finding only small variations in X-linked expression with no consistent pattern (Fig. 2, Table S2), showing that dosage compensation is maintained across tissues even under relaxed selection for up to 1.5 million years.

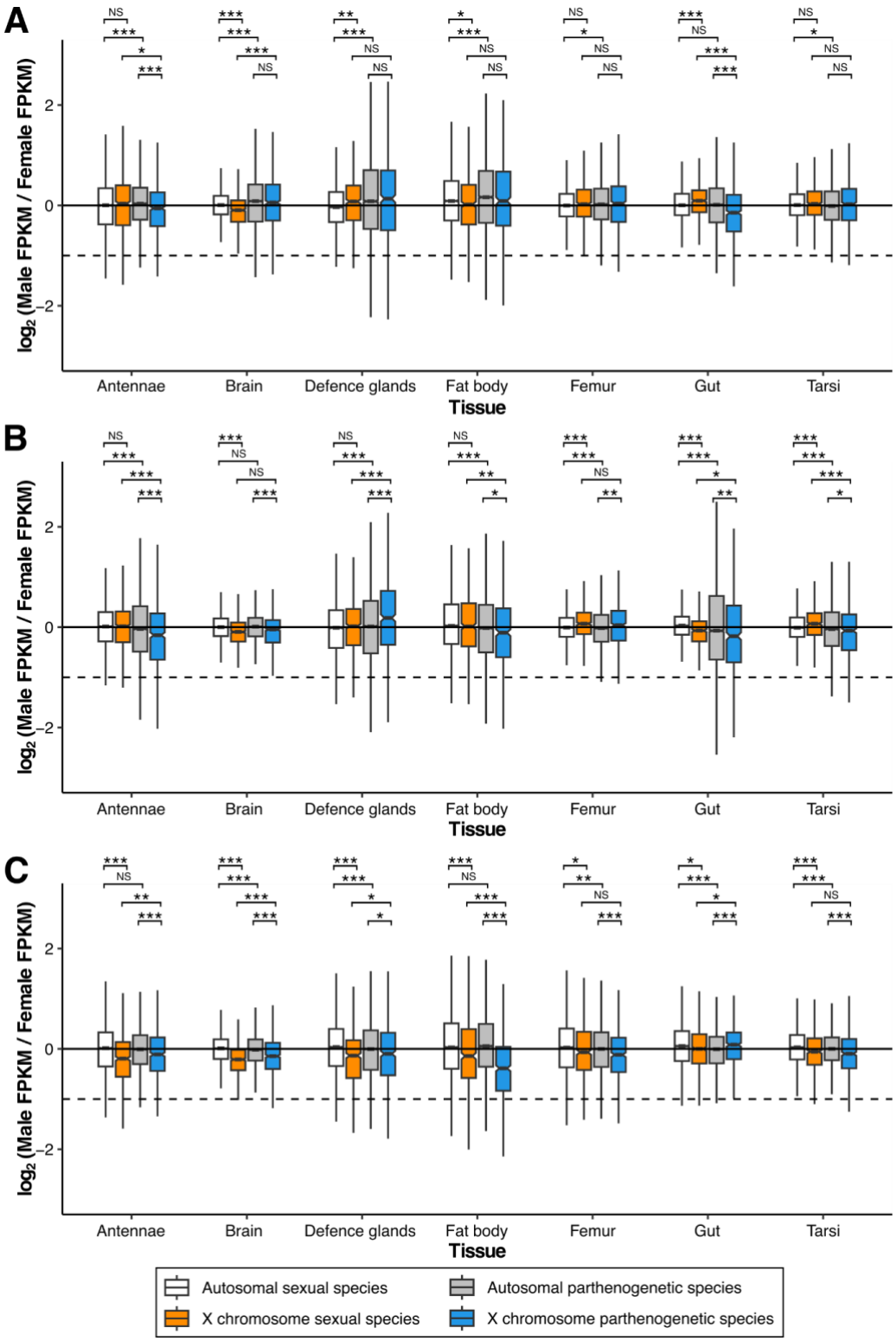

Fig. 2 | Male to female expression ratios for the X and autosomes in non-reproductive tissues reveal the maintenance of DC under relaxed selection. Dashed lines represent a two- fold reduction in expression in males (as expected if there was no dosage compensation). A. Sexual species = *T. cristinae*, parthenogenetic species = *T. monikense*. B. Sexual species = *T. podura*, parthenogenetic species = *T. genevievae.* C. Sexual species = *T. poppense*, parthenogenetic species = *T. douglasi.* Asterisks indicate the significance (FDR) of Wilcoxon tests (***<0.001, **<0.01, *<0.05, NS > 0.05).

Parthenogenetic species no longer need to perform dosage compensation as all individuals are female and carry the same number of sex chromosomes. Under this scenario, we would expect selection for a reduction in dosage compensation ability for two non-mutually exclusive reasons. Firstly, as the dosage compensation machinery is complex it is likely costly to produce and thus selection should act to remove it when it is no longer needed. One reason we do not observe any consistent changes may be that in insects most of the costs of producing dosage compensation machinery may be in males, as typically dosage compensation is achieved by hyper-transcribing the single X in males (Prince *et al.*, 2010; Conrad and Akhtar, 2012; Mahajan and Bachtrog, 2015; Rose *et al.*, 2016; Richard *et al.*, 2017). That said even if the cost to females was zero we may still expect to see a reduction in dosage composition ability due to the action of drift. We do not see this, which may mean that the genes involved in dosage compensation may be pleiotropic, and alterations therefore deleterious for females. Support for this idea stems from evidence for the maintenance of dosage compensation-like mechanisms targeting the ancestral X in *Drosophila melanogaster* fruit flies (Larsson *et al.*, 2004) even tens of myr after a sex chromosome turnover, which reverted the ancestral X back to an autosome (now referred to as the dot chromosome) (Vicoso and Bachtrog, 2015). Similar to our present study in parthenogenetic species, such reversals should result in relaxed selection for dosage compensation on the ancestral X/dot chromosome. Yet, the dot is regulated in a chromosome-specific manner via the protein POF (Larsson *et al.*, 2004), which might reflect vestiges of the former dosage compensation machinery when the dot was still the X chromosome.

A second reason to expect changes in dosage compensation could be if dosage compensation mechanisms result in maladaptive gene expression in females, i.e., partially unresolved sexual antagonism (Mank *et al.*, 2011). This factor may not have a strong influence in *Timema* as unresolved antagonisms are expected to be transient (Flintham *et al.*, 2025) yet the stick insect X chromosome is very old and highly conserved (Fig. 1) and shares most of its content with the X chromosome in other insect orders that diverged over 450 million years ago (Toups and Vicoso, 2023). Any maladaptive gene expression in females as a result of sexual conflict over dosage compensation would therefore be expected to be very small.

While our results show that dosage compensation is maintained in parthenogenetic species because selection against dosage compensation is weak or because changes to the underlying mechanisms are constrained, we cannot formally exclude that perhaps not enough time has passed since the evolution of parthenogenesis to observe any changes to dosage compensation. While this may be a likely explanation for dosage compensation maintenance across tissues in the young lineage *T. douglasi* and for the lack of apparent changes in dosage compensation in whole-body samples of males of parthenogenetic aphid lineages (Defendini *et al.*, 2025), it is very unlikely for the oldest species used here (*T. genevievae*) with an age estimate of over 1.5 million years (Schwander *et al.*, 2011; Bast *et al.*, 2018). This is likely ample time for even quite gradual changes in dosage compensation to be observed, especially given that *de novo* complete dosage compensation mechanisms can evolve in less than 4 million years (Metzger *et al.*, 2021).

A stronger signature of MSCI in parthenogenetic than sexual species driven by autosomal mis-expression during meiosis

We have shown previously that the X chromosome is consistently inactivated throughout male meiosis in sexual *Timema* species (Dumas *et al.*, 2024; Djordjevic *et al.*, 2025). Accordingly, we observe very low expression of X-linked genes in the testes, much lower than the expectation for a lack of dosage compensation (Fig. 3). We still observe some expression of the X in males, as expected given the presence of non-meiotic cells in testes. Surprisingly, we see a consistently lower expression of X-linked genes in males from parthenogenetic than sexual species (Fig. 3). This could indicate a higher proportion of meiotic cells in parthenogenetic than sexual males, or, more likely, that autosomal expression is more persistent across meiosis in parthenogenetic males.

To determine the dynamics of autosomal expression throughout meiosis in parthenogenetic males, we performed immunolabeling of testis tissue of *T. monikense* and *T. douglasi* using RNA polymerase II, a conserved transcriptional marker. In sexual *Timema* males, the X chromosome remains transcriptionally inactive throughout spermatogenesis, while there are two bursts of autosomal transcription during meiosis (Dumas *et al.*, 2024): a first at the end of prophase I (i.e., during pachytene and diplotene), and a second during meiosis II at the spermatid stage. An extension of the duration of these bursts could generate the observed decrease in X-linked expression in parthenogenetic males as compared to sexual males. We indeed observe such an extension as the RNA polymerase II signal already appears at the onset of prophase I (i.e., during the zygotene stage; Figs 4, S2) in males of both parthenogenetic species and is maintained until diplotene (Figs 4, S2).

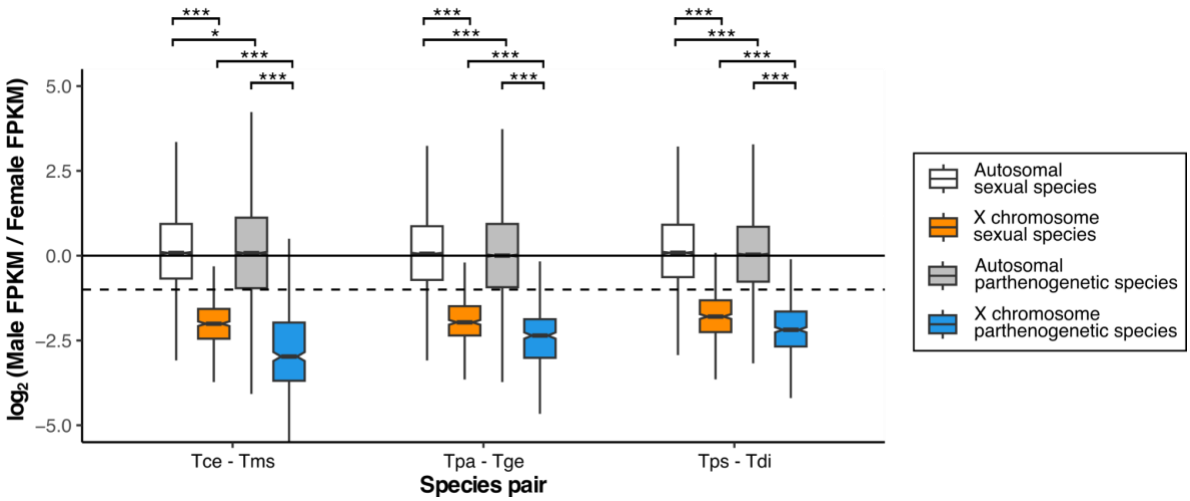

Fig. 3 | A stronger signature of MSCI in parthenogenetic than sexual species. Gene expression in reproductive tissues: Log_2 of male to female expression ratio for the X and autosomes in testes and female gonads. Species codes: Tce = *T. cristinae*, Tms = *T. monikense*, Tpa = *T. podura,* Tge = *T. genevievae,* Tps = *T. poppense* Tdi = *T. douglasi.* Asterisks indicate the significance (FDR) of Wilcoxon tests (***<0.001, **<0.01, *<0.05, NS > 0.05).

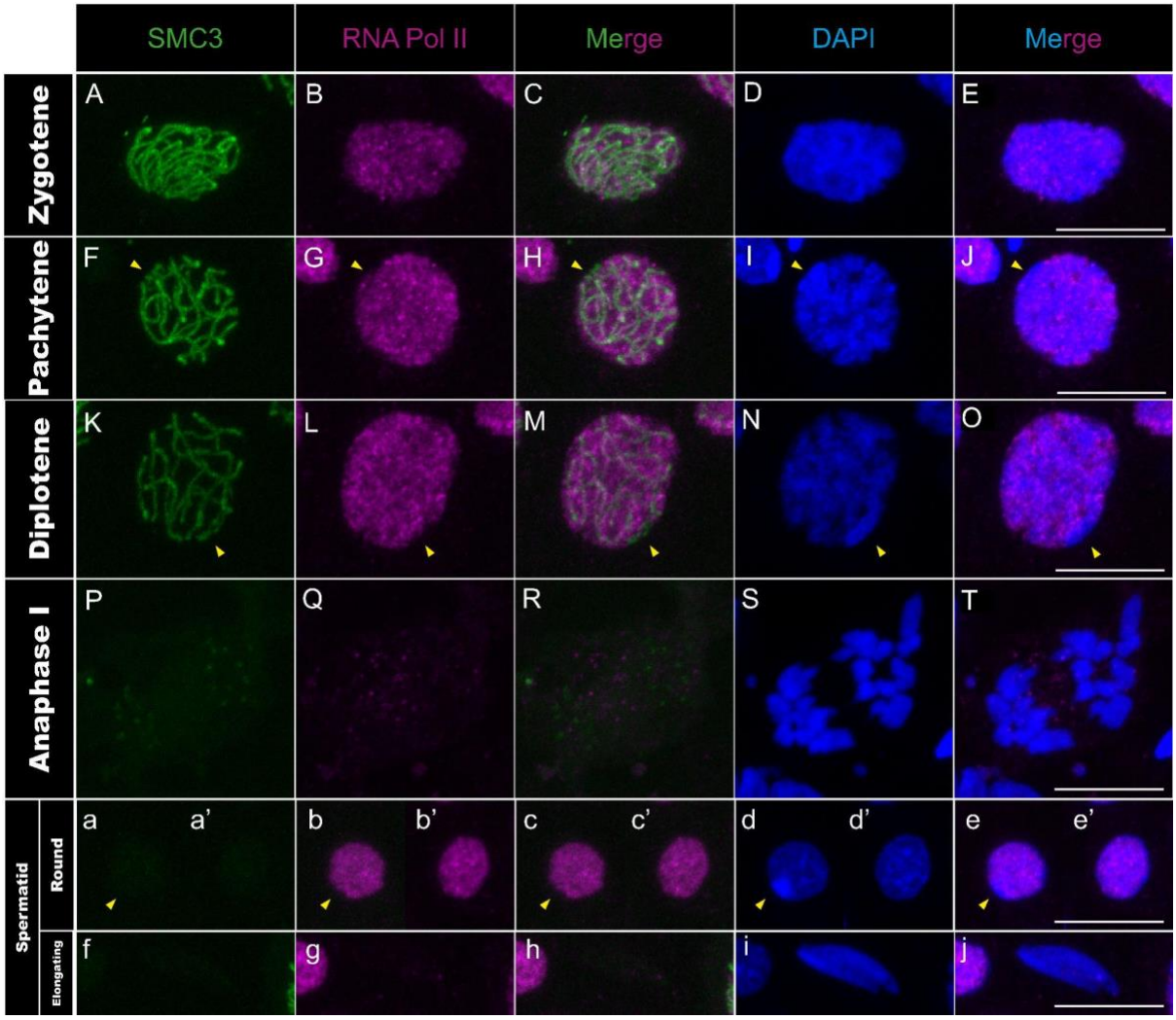

Fig. 4 | Misregulation of autosomal gene expression in meiotic cells of parthenogenetic males. RNApol-II distribution in *T. monikense* meiocytes and spermatids. Projections of stack images acquired across *T. monikense* squashed meiocytes (A–T) and spermatids (a–e'), at the stages indicated, stained with DAPI (blue) and double immunolabeled for SMC3 (green) and RNApol-II (magenta). RNApol-II labelling is intense from zygotene to diplotene, and in the round spermatid stage. During all spermatogenesis stages, the X chromosome is extremely reduced in RNApol-II labelling. The position of the X chromosome is indicated with arrowheads. Scale bar: 10 µm. Corresponding image analyses for males of *T. douglasi* are available in Fig. S2)

Conclusion

Our results demonstrate that both dosage compensation (DC) and meiotic sex chromosome inactivation (MSCI) are robustly maintained in parthenogenetic stick insects, despite the long-term absence of selective pressures typically associated with male phenotypes. This maintenance suggests that the molecular mechanisms underlying DC and MSCI are either functionally constrained, potentially due to pleiotropic effects in females, or maintained through weak purifying selection. Notably, the enhanced signature of MSCI in parthenogenetic males

251 appears to be driven by extended autosomal transcription during meiosis, revealing an
252 unexpected consequence of relaxed selection on gene expression. Together, these findings
253 highlight the stability and evolutionary inertia of complex regulatory processes, even in the
254 face of dramatic shifts in reproductive mode.

255 Methods

256 *Reference genome assemblies*

257
258 Reference genome assemblies were produced for *T. cristinae* (Bioproject PRJNA1268975/
259 Accession JBOIUC000000000) and *T. podura* (Bioproject PRJNA1268975/ Accession
260 JBOIUD000000000) from wild collected females (GPS coordinates 34°30'53.2"N,
261 119°46'45.3"W and 33°47'47.0"N, 116°46'34.6"W). Contigs for the *T. cristinae* assembly were
262 based on PacBio sequencing (43x) and on a combination of Nanopore and Illumina
263 sequencing for *T. podura* (sequenced at 85x respectively 62x coverage). Scaffolding was done
264 using a Hi-C library (sequenced at approximately 69 x and 53 x coverage for *T. cristinae* and
265 *T. podura* respectively) to produce the final reference assembly.
266
267 **DNA extraction and library preparation**
268
269 To extract high molecular weight (HMW) DNA, we flash-froze a single female (without gut) in
270 liquid nitrogen and ground it using a Cryomill (Retsch). We then extracted HMW DNA using
271 a G/20 Genomic Tips kit (Qiagen) following the manufacturer's protocols and checked DNA
272 integrity on a pulse field agarose gel.
273
274 For *T. cristinae*, a PacBio library was prepared using the Template Prep Kit 1.0 following
275 manufacturer's instructions and sequenced on a single cell of the PacBio SMRT™ system.
276 For T. podura, four ONT libraries were prepared following Oxford Nanopore instructions. A
277 first library was prepared using the SQK-LSK108 ligation sequencing kit and was loaded on a
278 MinION R9.4 Flow Cells, and then three libraries were prepared using the SQK-LSK109
279 ligation sequencing kit and were loaded on three PromethION R9.4.1 Flow Cells. A PCR free
280 Illumina library (based on the same HMW extraction) was prepared using the Kapa Hyper
281 Prep Kit (Roche, Basel, Switzerland), following manufacturer instructions. The library was
282 quantified by qPCR using the KAPA Library Quantification Kit for Illumina Libraries (Roche),
283 and the library profile was assessed using a High Sensitivity DNA kit on an Agilent Bioanalyzer
284 (Agilent Technologies, Santa Clara, CA, USA). The library was then sequenced on an Illumina
285 HiSeq 4000 instrument (Illumina, San Diego, CA, USA), using 150 base-length read chemistry
286 in a paired-end mode.
287
288 A Hi-C library was prepared for each species using the Proximo Hi-C Kit. We generated
289 ground tissue for cross-linking using Cryomill (Retsch) and following manufacturer
290 instructions, using a different female than the one used for Nanopore and HiSeq sequencing,
291 from the same natural population. Library construction and sequencing (250 million read pairs)
292 was outsourced to Phase Genomics (Seattle).

293 **Assembly pipelines**
294
295 We used different strategies for genome assembly for the two species. For *T. cristinae* raw
296 PacBio reads were assembled into contigs using Canu (Koren *et al.*, 2017) with the parameter
297 correctedErrorRate=0.105. For *T. podura* raw Oxford Nanopore reads were filtered using
298 Filtlong v0.2.0 (https://github.com/rrwick/Filtlong) with the parameters --min_length 1000 --
299 keep_percent 90 --target_bases 69050000000. The filtered Nanopore reads were then
300 assembled into contigs using Flye v2.8.1 (Kolmogorov *et al.*, 2019) with --genome-size 1.381g.
301 All Nanopore reads were mapped against the contigs using minimap2 v2.19 (Li, 2018) with
302 the parameters -c -x map-ont and a first step of polishing was performed using Racon v1.4.3
303 (Vaser *et al.*, 2017). Three additional rounds of polishing were conducted: Illumina short reads
304 were aligned to the contigs using BWA mem v0.7.17 (Li, 2013) and polishing was performed
305 using Pilon v1.23 (Walker *et al.*, 2014).
306
307 Both assemblies were then decontaminated using BlobTools v1.0 (Laetsch and Blaxter, 2017)
308 under the taxrule "bestsumorder". Hit files were generated after a blastn v2.10.1+ against the
309 NBCI nt database, searching for hits with an e-value below 1e-25 (parameters: -
310 max_target_seqs 10 -max_hsps 1 -evalue 1e-25). Contigs without hits to metazoans were
311 removed from the assemblies. Haplotypic duplications were then filtered out as follows.
312 Filtered reads were then mapped against the decontaminated genomes using minimap2 and
313 haplotigs were detected with Purge Haplotigs v1.1.1 (Roach *et al.*, 2018) using the parameters
314 -l 3 -m 27 -h 190 -j 101 --editor-coarse-resolution 250000 for *T. cristinae* and -l 3 -m 45 -h 195
315 -j 101 --editor-coarse-resolution 50000 for *T. podura*.
316
317 Hi-C reads from each species were then mapped against their respective haploid genome
318 using Juicer v1.6 (Durand *et al.*, 2016) with the restriction site Sau3AI. Finally, chromosome-
319 level scaffolding was performed using 3D-DNA v180922 (Dudchenko *et al.*, 2017) with
320 species-specific parameters, as recommended by the authors. The resulting Hi-C contact
321 matrices were visualized with Juicebox, and minor polishing was conducted in accordance
322 with these recommendations. The completeness of both genome assemblies was assessed
323 with BUSCO v5.1.2 (Seppey *et al.*, 2019) against the *insecta_odb10* dataset using the --long
324 and --augustus parameters.

325 ***Annotation***

326
327 We annotated the *T. cristinae* and *T. podura* genomes in a similar way as we previously
328 annotated the *T. poppense* genome (Djordjevic *et al.*, 2025), using a combination of *ab initio*
329 gene prediction, protein homology, and RNA-seq using the Braker2 pipeline (v. 2.1.6) (Brůna
330 *et al.*, 2021). Firstly, each genome assembly was soft-masked using RepeatModeler (v. 2.0.2,
331 options: -LTRStruct, -engine ncbi) (Flynn *et al.*, 2020) and RepeatMasker (v. 4.1.2, options: -
332 engine ncbi, -xsmall) (Smith *et al.*, 2013). For protein evidence, we used the arthropod protein
333 sequences from OrthoDB (v.10.1) (Kriventseva *et al.*, 2019) and the predicted protein
334 sequences for *Timema* from our previous genome assemblies. For RNAseq evidence, we
335 used the RNAseq libraries generated here for *T. cristinae* and *T. monikense* along with publicly
336 available data (163 libraries generated here, 43 public (Bioproject accessions: PRJNA380865,
337 PRJNA679785, PRJNA1295360, PRJNA504764 (Bast *et al.*, 2018; Parker *et al.*, 2019; Jaron
338 *et al.*, 2022))) to annotate the *T. cristinae* genome and for *T. podura* and *T. genevievae* (119

339 libraries generated here, 29 public (Bioproject accessions: PRJNA380865, PRJNA679785,
340 PRJNA1295360 (Bast *et al.*, 2018; Jaron *et al.*, 2022))) to annotate the *T. podura* genome.
341 This is a total of 354 RNAseq libraries (330 paired-end, 24 single-end) covering over 19
342 different life stages, tissue, and sex combinations for each species (see Table S3). Reads
343 were quality trimmed with Trimmomatic (v. 0.39, options: ILLUMINACLIP:3:25:6 LEADING:9
344 TRAILING:9 SLIDINGWINDOW:4:15 MINLEN:80) (Bolger *et al.*, 2014) before mapping to the
345 genome assembly with STAR (v. 2.7.8a, options: --twopassMode Basic) (Dobin *et al.*, 2013).
346 Braker2 was run using protein evidence and RNAseq separately with the gene predictors
347 Augustus (v. 3.4.0) (Stanke *et al.*, 2006) and Genemark (v. 4.72) (Brůna *et al.*, 2020).
348 Following the RNAseq run, UTR predictions were added to the RNAseq gene predictions using
349 GUSHR (v. 1.0) in Braker2 (--addUTR=on). The separate gene predictions were then merged
350 using TSEBRA (v1.0.3) using the pref_braker1.cfg configuration file, which weights RNAseq
351 evidence more strongly than the default option. We then ran BUSCO (v. 5.3.2, insecta_odb10)
352 on the gene regions annotated by Braker2 and on the whole genome assembly. Any genes
353 found by BUSCO but missed by Braker were then added to the annotation (69 genes for *T.*
354 *cristinae* and 19 genes for *T. podura*). ncRNA genes were predicted using Infernal (v. 1.1.2,
355 minimum e-value 1e-10) (Nawrocki and Eddy, 2013). GO-terms for protein-coding gene
356 predictions were obtained using blastP within OmicsBox (v3.1.2, default parameters) to blast
357 the nr *Drosophila melanogaster* database (taxonomy filter: 7227). 1-to-1 orthologs between
358 were obtained for protein-coding genes using OrthoFinder (version 2.5.5) (Emms and Kelly,
359 2019) with default options.

360 ***Identification of the X chromosome***

361

362 We used a coverage approach to identify X-linked scaffolds in our new genome assemblies.
363 To do this we mapped publicly available Illumina genome reads from males and females (4
364 males and 5 females for *T. cristinae* and 4 males and 2 females for *T. podura* (PRJNA670663,
365 PRJNA725673 (Jaron *et al.*, 2022; Parker *et al.*, 2022)) to the respective genome assemblies
366 using BWA-MEM (v. 0.7.15). Multi- mapping and poor quality alignments were filtered
367 (removing reads with XA:Z or SA:Z tags or a mapq <30). PCR duplicates were removed with
368 Picard (v. 2.9.0) (http://broadinstitute.github.io/picard/). Coverage was then estimated for
369 100000 bp sliding windows using BEDTools (v. 2.26.0) (Quinlan and Hall, 2010). To compare
370 coverage between males and females, coverage was first summed for all male and all female
371 libraries per window. Male and female coverage was then normalized by modal coverage to
372 adjust for differences in overall coverage. X- linked windows were then identified using the
373 $\log_2$ ratio of male to female coverage. Autosomal windows should have equal coverage in
374 males and females ($\log_2$ ratio of male to female coverage ≈ 0) and X-linked windows should
375 have half the coverage in males as in females ($\log_2$ ratio of male to female coverage ≈ -1).
376 This approach identified one large scaffold in each assembly as the X chromosome (Fig. S3-
377 5).
378

379 We then repeated these analyses using genome reads from each of the parthenogenetic
380 species. Female reads were publicly available (5 for *T. monikense*, 6 for *T. genevievae*, and
381 5 for *T. douglasi*, PRJNA670663 (Jaron *et al.*, 2022)) as were the two male samples for *T.*
382 *douglasi* (PRJNA808673, (Larose *et al.*, 2022)). For *T. monikense* and *T. genevievae* we also
383 generated new Illumina libraries for males (2 for *T. genevievae* and 4 for *T. monikense*) and
384 an additional female library for *T. genevievae* (Accession number: PRJNA1293928) as

385 described previously (Jaron *et al.*, 2022) using the carcasses after tissue dissection described
386 below. Reads were then mapped to the genome of each sexual sister species as described
387 above. Each of the newly generated samples were checked for normal coverage distributions
388 before calculating coverage ratios.
389

390 ***RNA extraction and sequencing***

391
392 We generated a total of 282 RNA-seq libraries for eight female tissues (antennae, brain,
393 defence glands, fat body, femur, tarsi, and gonads) and nine male tissues (the same as the
394 female plus the male accessory glands) for *T. cristinae*, *T. podura*, *T. monikense*, and *T.*
395 *genevievae* following our previously developed methodology (Djordjevic *et al.*, 2025) (see
396 Table S3 for details). Individuals were collected as nymphs in the field and reared to adulthood
397 in the laboratory. Prior to dissection all individuals were isolated in Petri dishes and fed on an
398 artificial diet (a mix of flour, sugar, and water) for two days, allowing their gut contents to be
399 cleared of plant material. Insects were then anesthetized with CO_2, dissected, and tissues
400 individually flash-frozen in liquid nitrogen before being stored at -80°C.
401
402 TRIzol solution (1 mL) and a small amount of ceramic beads (Sigmund Lindner) were added
403 to each tissue. Samples were homogenized using a tissue homogenizer (Precellys Evolution;
404 Bertin Technologies). Chloroform (200 µL) was added to each sample and samples were then
405 vortexed for 15 seconds and centrifuged for 25 minutes at 12,000 rpm at 4°C. The upper
406 phase containing the RNA was then transferred to a new 1.5 mL tube with the addition of
407 isopropanol (650 µL). The samples were vortexed and placed at -20°C overnight. Samples
408 were then centrifuged for 30 minutes at 12,000 rpm at 4°C. The liquid supernatants were
409 removed, and the RNA pellet underwent two washes using 80% and 70% ethanol. Each wash
410 was followed by a 5-minute centrifugation step at 12,000 rpm. Finally, the RNA pellet was
411 resuspended in nuclease-free water and quantified using a fluorescent RNA-binding dye
412 (QuantiFluor RNA System) and nanodrop (DS-11 FX).
413
414 Library preparation using NEBNext (New England BioLabs) and sequencing on an Illumina
415 NovaSeq 6000 platform with 100 bp paired-end sequencing (36.2 million read pairs per
416 sample on average) was outsourced to a sequencing facility (Fasteris, Geneva).

417 ***Gene expression analyses***

418
419 We mapped RNAseq reads from *T. cristinae*, *T. podura*, *T. monikense*, and *T. genevievae*
420 generated here and reads for *T. poppense* and *T. douglasi* we generated previously
421 (Djordjevic *et al.*, 2025) to their respective genomes as described above. This gave 4
422 replicates for each of the 16 sex and tissue combinations for each of the six species, except
423 for the male samples of parthenogenetic species (*T. monikense, T. genevievae,* and *T.*
424 *douglasi*) where we had fewer replicates due to the difficulty of obtaining these specimens (n
425 = 2-4 see Table S4 for details). Read counts were obtained using HTSeq v.0.9.1 (Anders *et*
426 *al.*, 2015), with the following options (htseq-count --order = name --type = exon --idattr =
427 gene_id --stranded = reverse). Expression analyses were performed using the Bioconductor
428 package EdgeR (v 3.42.4) (Robinson *et al.*, 2010), and done separately for each species and
429 tissue. Normalization factors for each library were computed using the TMM method and were

430 used to calculate normalized expression levels (FPKM, Fragments Per Kilobase of transcript
431 per Million mapped reads). mtDNA, rRNA, tRNA and genes with low expression (less than 2
432 FPKM in 2 or more libraries per sex) were excluded. To examine dosage compensation, we
433 used the $\log_2$ ratio of mean male expression level to female expression level and used
434 Wilcoxon tests (adjusted for multiple testing using Benjamini and Hochberg's (1995) algorithm)
435 to determine if differences in expression between the autosomes and the X chromosome were
436 significant.
437
438 ***Immunolabeling of parthenogenetic male meiotic cells***
439
440 In order to determine the dynamics of autosomal gene expression during meiosis in
441 parthenogenetic males, we followed the same protocol previously used to characterize
442 autosomal gene expression during meiosis in sexual males (Dumas *et al.*, 2024). In brief, we
443 performed double immunolabeling of SMC3_488 (#AB201542, AbCam) as a marker of
444 cohesin axes (this allows for the assessment of synapsis progression, and hence, cell cycle
445 stage) and RNA polymerase II phosphorylated at serine 2 (p-RNApol-II (ab193468, AbCam);
446 an indicator of transcription). Gonads from adult *T. monikense* and *T. douglasi* males were
447 dissected in 1X PBS, then fixed in paraformaldehyde (2%) and Triton X-100 (0.1%) solution
448 for 15 minutes. Gonads were then squashed on slides coated with poly-L-lysine, and flash
449 frozen in liquid nitrogen. Slides were incubated in PBS 1x for 20 minutes at room temperature,
450 then blocked with a BSA 3% solution (prepared by dissolving 3g of BSA in 100mL of PBS 1X)
451 for 20 minutes. Slides were then incubated overnight at 4°C in a humid chamber with the
452 primary (p-RNA-Pol II), diluted in BSA 3% (1:100), and washed 3x for 5 minutes in PBS 1X.
453 The secondary antibody, anti-rabbit Alexa 594 (711-585-152, Jackson), diluted in BSA 3%
454 (1:100), was applied, and samples were incubated for 45 minutes at room temperature.
455 Further washes were conducted as described above, followed by an extended 10-minute wash
456 in PBS 1X, and by blocking using a 5% Normal Rabbit Serum (NRS) solution (X090210-8,
457 Agilent Technology) for 30 minutes at room temperature. Another 5-minute wash in PBS 1x
458 was performed to remove excess blocking solution. Samples were then incubated with the
459 labelled antibody SMC3_488 (#AB201542, AbCam) at a 1:100 dilution for 1 hour at room
460 temperature, followed by a final series of washes and staining with DAPI (D9542, Sigma-
461 Aldrich) for 3 minutes at room temperature. Finally, after a 5-minute wash in 1x PBS, two drops
462 of Vectashield were added to the slide, which was then covered with a coverslip, and sealed
463 with nail varnish for imaging. Image acquisition was performed at the Cellular Imaging Facility
464 (CIF, University of Lausanne) using a Zeiss LSM 880 Airyscan.

Data

Genome assemblies have been deposited at DDBJ/ENA/GenBank under the accessions JBOIUC000000000 (*T. cristinae*) and JBOIUD000000000 (*T. podura*). The Illumina and PromethION sequencing data for *T. podura* are available in the European Nucleotide Archive under the following project PRJEB94285. Male genomic reads have been deposited at SRA under the following project PRJNA1293928. Code will be deposited here: https://github.com/DarrenJParker/Timema_DC_MSCI_code

Acknowledgments

This work was supported by the European Research Council Consolidator Grant 864672 ("No Sex No Conflict", T.S.), Swiss FNS grant 31003A_182495 (T.S.), the Genoscope, the Commissariat à l'Énergie Atomique et aux Énergies Alternatives (CEA) and France Génomique (ANR-10-INBS-09–08). Lausanne Genomic Technologies Facility for PacBio and RNA library preparation and sequencing.

References

Anders S, Pyl PT, Huber W (2015). HTSeq--a Python framework to work with high-throughput sequencing data. *Bioinformatics* **31**: 166–169.

Bank S, Bradler S (2022). A second view on the evolution of flight in stick and leaf insects (Phasmatodea). *BMC Ecol Evol* **22**: 62.

Bast J, Parker DJ, Dumas Z, Jalvingh KM, Tran Van P, Jaron KS, *et al.* (2018). Consequences of asexuality in natural populations: insights from stick insects. *Mol Biol Evol* **35**: 1668–1677.

Benjamini Y, Hochberg Y (1995). Controlling the false discovery rate: A practical and powerful approach to multiple testing. *J R Stat Soc Series B Stat Methodol* **57**: 289–300.

Bolger AM, Lohse M, Usadel B (2014). Trimmomatic: a flexible trimmer for Illumina sequence data. *Bioinformatics* **30**: 2114–2120.

Brockdorff N, Turner BM (2015). Dosage compensation in mammals. *Cold Spring Harb Perspect Biol* **7**: a019406.

Brůna T, Hoff KJ, Lomsadze A, Stanke M, Borodovsky M (2021). BRAKER2: automatic eukaryotic genome annotation with GeneMark-EP+ and AUGUSTUS supported by a protein database. *NAR Genom Bioinform* **3**: lqaa108.

Brůna T, Lomsadze A, Borodovsky M (2020). GeneMark-EP+: eukaryotic gene prediction with self-training in the space of genes and proteins. *NAR Genom Bioinform* **2**: lqaa026.

Chauhan P, Swaegers J, Guillen RAS, Svensson EI, Wellenreuther M, Hansson B (2021). Genome assembly, sex-biased gene expression and dosage compensation in the damselfly *Ischnura elegans*. *Genomics* **113**: 1828–1837.

Conrad T, Akhtar A (2012). Dosage compensation in *Drosophila melanogaster*: epigenetic fine-tuning of chromosome-wide transcription. *Nat Rev Genet* **13**: 123–134.

Darolti I, Wright AE, Sandkam BA, Morris J, Bloch NI, Farré M, *et al.* (2019). Extreme heterogeneity in sex chromosome differentiation and dosage compensation in livebearers. *Proc Natl Acad Sci U S A* **116**: 19031–19036.

Davis RJ, Belikoff EJ, Scholl EH, Li F, Scott MJ (2018). No blokes is essential for male viability and X chromosome gene expression in the Australian sheep blowfly. *Curr Biol* **28**: 1987–1992.e3.

Defendini H, Prunier-Leterme N, Robin S, Lameiras S, Baulande S, Simon J-C, *et al.* (2025). The release of sexual conflict after sex loss is associated with evolutionary changes in gene expression. *Proc Biol Sci* **292**: 20242631.

Disteche CM (2012). Dosage compensation of the sex chromosomes. *Annu Rev Genet* **46**: 537–560.

Djordjevic J, Tran Van P, Toubiana W, Labédan M, Dumas Z, Aury J-M, *et al.* (2025). Dynamics of X chromosome hyper-expression and inactivation in male tissues during stick insect development. *PLoS Genet* **21**: e1011615.

Dobin A, Davis CA, Schlesinger F, Drenkow J, Zaleski C, Jha S, *et al.* (2013). STAR: ultrafast universal RNA-seq aligner. *Bioinformatics* **29**: 15–21.

518 Dudchenko O, Batra SS, Omer AD, Nyquist SK, Hoeger M, Durand NC, *et al.* (2017). De novo
519 assembly of the Aedes aegypti genome using Hi-C yields chromosome-length scaffolds.
520 *Science* **356**: 92–95.

521 Dumas Z, Toubiana W, Delattre M, Schwander T (2024). Dynamics of recombination, X
522 inactivation and centromere proteins during stick insect spermatogenesis. *bioRxiv*:
523 2024.09.05.611401.

524 Durand NC, Shamim MS, Machol I, Rao SSP, Huntley MH, Lander ES, *et al.* (2016). Juicer
525 provides a one-click system for analyzing loop-resolution Hi-C experiments. *Cell Syst* **3**:
526 95–98.

527 Emms DM, Kelly S (2019). OrthoFinder: phylogenetic orthology inference for comparative
528 genomics. *Genome Biol* **20**: 238.

529 Flintham E, Savolainen V, Otto SP, Reuter M, Mullon C (2025). The maintenance of genetic
530 polymorphism underlying sexually antagonistic traits. *Evol Lett* **9**: 259–272.

531 Flynn JM, Hubley R, Goubert C, Rosen J, Clark AG, Feschotte C, *et al.* (2020).
532 RepeatModeler2 for automated genomic discovery of transposable element families. *Proc*
533 *Natl Acad Sci U S A* **117**: 9451–9457.

534 Freitas S, Parker DJ, Labédan M, Dumas Z, Schwander T (2023). Evidence for cryptic sex in
535 parthenogenetic stick insects of the genus Timema. *Proceedings of the Royal Society B:*
536 *Biological Sciences* **290**: 20230404.

537 Gu L, Walters JR (2017). Evolution of sex chromosome dosage compensation in animals: a
538 beautiful theory, undermined by facts and bedeviled by details. *Genome Biol Evol* **9**:
539 2461–2476.

540 Hamada FN, Park PJ, Gordadze PR, Kuroda MI (2005). Global regulation of X chromosomal
541 genes by the MSL complex in Drosophila melanogaster. *Genes Dev* **19**: 2289–2294.

542 Hu Q-L, Ye Y-X, Zhuo J-C, Huang H-J, Li J-M, Zhang C-X (2022). Chromosome-level
543 assembly, dosage compensation and sex-biased gene expression in the small brown
544 planthopper, Laodelphax striatellus. *Genome Biol Evol* **14**: evac160.

545 Jaron KS, Parker DJ, Anselmetti Y, Van PT, Bast J, Dumas Z, *et al.* (2022). Convergent
546 consequences of parthenogenesis on stick insect genomes. *Science Advances* **8**:
547 eabg3842.

548 Kalita AI, Keller Valsecchi CI (2024). Dosage compensation in non-model insects - progress
549 and perspectives. *Trends Genet*.

550 Kalita AI, Marois E, Kozielska M, Weissing FJ, Jaouen E, Möckel MM, *et al.* (2023). The sex-
551 specific factor SOA controls dosage compensation in Anopheles mosquitoes. *Nature* **623**:
552 175–182.

553 Kelley RL, Solovyeva I, Lyman LM, Richman R, Solovyev V, Kuroda MI (1995). Expression of
554 msl-2 causes assembly of dosage compensation regulators on the X chromosomes and
555 female lethality in Drosophila. *Cell* **81**: 867–877.

556 Kolmogorov M, Yuan J, Lin Y, Pevzner PA (2019). Assembly of long, error-prone reads using
557 repeat graphs. *Nat Biotechnol* **37**: 540–546.

558 Koren S, Walenz BP, Berlin K, Miller JR, Bergman NH, Phillippy AM (2017). Canu: scalable
559 and accurate long-read assembly via adaptive k-mer weighting and repeat separation.

560 *Genome Res* **27**: 722–736.

561 Kriventseva EV, Kuznetsov D, Tegenfeldt F, Manni M, Dias R, Simão FA, *et al.* (2019).
562 OrthoDB v10: sampling the diversity of animal, plant, fungal, protist, bacterial and viral
563 genomes for evolutionary and functional annotations of orthologs. *Nucleic Acids Res* **47**:
564 D807–D811.

565 Krzywinska E, Ribeca P, Ferretti L, Hammond A, Krzywinski J (2023). A novel factor
566 modulating X chromosome dosage compensation in Anopheles. *Curr Biol* **33**: 4697–
567 4703.e4.

568 Laetsch DR, Blaxter ML (2017). BlobTools: Interrogation of genome assemblies. *F1000Res*
569 **6**: 1287.

570 Larose C, Lavanchy G, Freitas S, Parker DJ, Schwander T (2022). Facultative
571 parthenogenesis in an asexual stick insect: re-evolution of sex or vestigial sexual
572 capacity? *bioRxiv*: 2022.03.25.485836.

573 Larsson J, Svensson MJ, Stenberg P, Mäkitalo M (2004). Painting of fourth in genus
574 Drosophila suggests autosome-specific gene regulation. *Proc Natl Acad Sci U S A* **101**:
575 9728–9733.

576 Lee JT (2000). Disruption of imprinted X inactivation by parent-of-origin effects at Tsix. *Cell*
577 **103**: 17–27.

578 Li H (2013). Aligning sequence reads, clone sequences and assembly contigs with BWA-
579 MEM. *arXiv*: 1303.3997.

580 Li H (2018). Minimap2: pairwise alignment for nucleotide sequences. *Bioinformatics* **34**: 3094–
581 3100.

582 Li X, Mank JE, Ban L (2024). The grasshopper genome reveals long-term gene content
583 conservation of the X Chromosome and temporal variation in X Chromosome evolution.
584 *Genome Res* **34**: 997–1007.

585 Mahajan S, Bachtrog D (2015). Partial dosage compensation in Strepsiptera, a sister group of
586 beetles. *Genome Biol Evol* **7**: 591–600.

587 Mank JE (2013). Sex chromosome dosage compensation: definitely not for everyone. *Trends*
588 *Genet* **29**: 677–683.

589 Mank JE, Hosken DJ, Wedell N (2011). Some inconvenient truths about sex chromosome
590 dosage compensation and the potential role of sexual conflict. *Evolution* **65**: 2133–2144.

591 Marin R, Cortez D, Lamanna F, Pradeepa MM, Leushkin E, Julien P, *et al.* (2017). Convergent
592 origination of a Drosophila-like dosage compensation mechanism in a reptile lineage.
593 *Genome Res* **27**: 1974–1987.

594 McKee BD, Handel MA (1993). Sex chromosomes, recombination, and chromatin
595 conformation. *Chromosoma* **102**: 71–80.

596 Metzger DCH, Sandkam BA, Darolti I, Mank JE (2021). Rapid Evolution of Complete Dosage
597 Compensation in Poecilia. *Genome Biol Evol* **13**.

598 Meyer BJ (2000). Sex in the worm: counting and compensating X-chromosome dose. *Trends*
599 *Genet* **16**: 247–253.

600 Namekawa SH, Lee JT (2009). XY and ZW: is meiotic sex chromosome inactivation the rule
601 in evolution? *PLoS Genet* **5**: e1000493.

602 Nawrocki EP, Eddy SR (2013). Infernal 1.1: 100-fold faster RNA homology searches.
603 *Bioinformatics* **29**: 2933–2935.

604 Page N, Taxiarchi C, Tonge D, Kuburic J, Chesters E, Kriezis A, *et al.* (2023). Single-cell
605 profiling of Anopheles gambiae spermatogenesis defines the onset of meiotic silencing
606 and premeiotic overexpression of the X chromosome. *Commun Biol* **6**: 850.

607 Pal A, Vicoso B (2015). The X Chromosome of Hemipteran insects: conservation, dosage
608 compensation and sex-biased expression. *Genome Biol Evol* **7**: 3259–3268.

609 Parker DJ, Djordjevic J, Schwander T (2019). Olfactory proteins in *Timema* stick insects.
610 *Frontiers in Ecology and Evolution* **7**: 101.

611 Parker DJ, Jaron KS, Dumas Z, Robinson-Rechavi M, Schwander T (2022). X chromosomes
612 show relaxed selection and complete somatic dosage compensation across Timema stick
613 insect species. *J Evol Biol*.

614 Pease JB, Hahn MW (2012). Sex chromosomes evolved from independent ancestral linkage
615 groups in winged insects. *Mol Biol Evol* **29**: 1645–1653.

616 Prince EG, Kirkland D, Demuth JP (2010). Hyperexpression of the X chromosome in both
617 sexes results in extensive female bias of X-linked genes in the flour beetle. *Genome Biol*
618 *Evol* **2**: 336–346.

619 Quinlan AR, Hall IM (2010). BEDTools: a flexible suite of utilities for comparing genomic
620 features. *Bioinformatics* **26**: 841–842.

621 Rayner JG, Hitchcock TJ, Bailey NW (2021). Variable dosage compensation is associated
622 with female consequences of an X-linked, male-beneficial mutation. *Proc Biol Sci* **288**:
623 20210355.

624 Richard G, Legeai F, Prunier-Leterme N, Bretaudeau A, Tagu D, Jaquiéry J, *et al.* (2017).
625 Dosage compensation and sex-specific epigenetic landscape of the X chromosome in the
626 pea aphid. *Epigenetics Chromatin* **10**: 30.

627 Roach MJ, Schmidt SA, Borneman AR (2018). Purge Haplotigs: allelic contig reassignment
628 for third-gen diploid genome assemblies. *BMC Bioinformatics* **19**: 460.

629 Robinson MD, McCarthy DJ, Smyth GK (2010). edgeR: a Bioconductor package for differential
630 expression analysis of digital gene expression data. *Bioinformatics* **26**: 139–140.

631 Rose G, Krzywinska E, Kim J, Revuelta L, Ferretti L, Krzywinski J (2016). Dosage
632 compensation in the African Malaria Mosquito *Anopheles gambiae*. *Genome Biol Evol* **8**:
633 411–425.

634 Schoenmakers S, Wassenaar E, Hoogerbrugge JW, Laven JSE, Grootegoed JA, Baarends
635 WM (2009). Female meiotic sex chromosome inactivation in chicken. *PLoS Genet* **5**:
636 e1000466.

637 Schwander T, Crespi BJ (2009). Multiple direct transitions from sexual reproduction to
638 apomictic parthenogenesis in *Timema* stick insects. *Evolution* **63**: 84–103.

639 Schwander T, Crespi BJ, Gries R, Gries G (2013). Neutral and selection-driven decay of
640 sexual traits in asexual stick insects. *Proc Biol Sci* **280**: 20130823.

641 Schwander T, Henry L, Crespi BJ (2011). Molecular evidence for ancient asexuality in *Timema*
642 stick insects. *Curr Biol* **21**: 1129–1134.

643 Seppey M, Manni M, Zdobnov EM (2019). BUSCO: Assessing genome assembly and
644 annotation completeness. *Methods Mol Biol* **1962**: 227–245.

645 Smith A, Hubley R, Green P (2013). RepeatMasker Open-4.0. *RepeatMasker Open-40*.

646 Stanke M, Keller O, Gunduz I, Hayes A, Waack S, Morgenstern B (2006). AUGUSTUS: ab
647 initio prediction of alternative transcripts. *Nucleic Acids Res* **34**: W435–9.

648 Straub T, Gilfillan GD, Maier VK, Becker PB (2005). The Drosophila MSL complex activates
649 the transcription of target genes. *Genes Dev* **19**: 2284–2288.

650 Toups MA, Vicoso B (2023). The X chromosome of insects likely predates the origin of class
651 Insecta. *Evolution* **77**: 2504–2511.

652 Toups MA, Vicoso B (2025). Insect sex chromosome evolution: conservation, turnover, and
653 mechanisms of dosage compensation. *Curr Opin Insect Sci*: 101411.

654 Vaser R, Sović I, Nagarajan N, Šikić M (2017). Fast and accurate de novo genome assembly
655 from long uncorrected reads. *Genome Res* **27**: 737–746.

656 Vicoso B, Bachtrog D (2015). Numerous transitions of sex chromosomes in Diptera. *PLoS Biol*
657 **13**: e1002078.

658 Walker BJ, Abeel T, Shea T, Priest M, Abouelliel A, Sakthikumar S, *et al.* (2014). Pilon: an
659 integrated tool for comprehensive microbial variant detection and genome assembly
660 improvement. *PLoS One* **9**: e112963.